

The color dipole model bounds with the gluon-gluon recombination correction

G.R.Boroun* and B.Rezaei†

Physics Department, Razi University, Kermanshah 67149, Iran

(Dated: October 12, 2021)

We present nonlinear (NL) and higher twist (HT) corrections to the color dipole model (CDM) bounds at low values of x and Q^2 using the parameterization method. Consistency between the bounds at this region describe that a transition from the linear to the nonlinear behavior is dependence on the behavior of the gluon distribution function. The parameters in the color dipole model are comparable with the color dipole bounds at low values of Q^2 . Consequently, the obtained reduced cross sections at low and moderate Q^2 values due to the NL+HT effects show a good agreement with the H1 data.

1. Introduction

The starting points on the color dipole model were given by Sakurai and Schildknecht in 1972 [1] and has been expanded so far by some authors in Refs.[2,3,4]. The modern picture of the deep inelastic scattering (DIS) at low x is described as the color dipole picture (CDP). In this picture the virtual photon fluctuates into the $q\bar{q}$ pair which this pair interaction with the gluon field in the nucleon as a gauge-invariant color-dipole interaction. Due to the interaction of the gluon fields with the $q\bar{q}$ dipole, the dipole cross section, $\sigma_{(q\bar{q})_{L,T}^{\perp=1}p}$, is described at the color transparency and saturation limits. The W^2 -dependent scale $\Lambda_{sat}^2(W^2)$ separates the two regions. The color transparency of the dipole cross section according to the region of $Q^2 \gg \Lambda_{sat}^2(W^2)$ and the saturation according to the region of $Q^2 \ll \Lambda_{sat}^2(W^2)$ respectively. Indeed the (Q^2, W^2) plane of the CDP indicates that the line $\eta(W^2, Q^2) = 1$ subdivides the (Q^2, W^2) plane into the saturation region of $\eta(W^2, Q^2) < 1$ and the color transparency region of $\eta(W^2, Q^2) > 1$. $\eta(W^2, Q^2)$ denotes the low- x scaling variable, $\eta(W^2, Q^2) = \frac{Q^2 + m_0^2}{\Lambda_{sat}^2(W^2)}$ which $\Lambda_{sat}^2(W^2)$ being the saturation scale and $m_0^2 \simeq 0.15 \text{ GeV}^2$. At low- x scaling, the total photoabsorption cross section $\sigma_{\gamma^*p}(W^2, Q^2) = \sigma_{\gamma^*p}(\eta(W^2, Q^2))$ is described as $\log(1/\eta(W^2, Q^2))$ for $\eta(W^2, Q^2) < 1$ and as $1/\eta(W^2, Q^2)$ for $\eta(W^2, Q^2) \gg 1$. At large $Q^2 \gg \Lambda_{sat}^2(W^2)$, the longitudinal-to-transverse ratio of the photoabsorption cross sections $\sigma_{\gamma_{LP}^*}(W^2, Q^2)$ and $\sigma_{\gamma_{TP}^*}(W^2, Q^2)$ reads as

$$R(W^2, Q^2) = \frac{\sigma_{\gamma_{LP}^*}(W^2, Q^2)}{\sigma_{\gamma_{TP}^*}(W^2, Q^2)} = \frac{1}{2\rho}. \quad (1)$$

In terms of the proton structure functions, the ratio of the structure functions becomes

$$\frac{F_L(W^2, Q^2)}{F_2(W^2, Q^2)} = \frac{1}{1 + 2\rho}. \quad (2)$$

The parameter ρ is associated with the enhanced transverse size of $q\bar{q}$ fluctuations in the CDM. This parameter is originating from transverse, $\gamma_T^* \rightarrow q\bar{q}$, and longitudinal, $\gamma_L^* \rightarrow q\bar{q}$, photons. Indeed the ρ parameter describes the ratio of the average transverse momenta $\rho = \frac{\langle \vec{k}_\perp^2 \rangle_L}{\langle \vec{k}_\perp^2 \rangle_T}$. It can also be related to the ratio of the effective transverse sizes of the $(q\bar{q})_{L,T}^{J=1}$ states as $\frac{\langle \vec{r}_\perp^2 \rangle_L}{\langle \vec{r}_\perp^2 \rangle_T} = \frac{1}{\rho}$. The ρ parameter is assumed to be proportional to the singlet structure and gluon distribution functions in the large- Q^2 limit [5]

$$\rho(x, Q^2) = \frac{3\pi}{8\alpha_s(Q^2)} \frac{F_2^s(x, Q^2)}{G(x, Q^2)} - \frac{1}{2}, \quad (3)$$

where $F_2^s(x, Q^2) = x\Sigma(x, Q^2)$ and $G(x, Q^2) = xg(x, Q^2)$. In this paper we want to show that the behavior of the CDM bounds at low and moderate Q^2 values are depends on the gluon density behavior. In this case the bounds are obtained via the nonlinear-DGLAP (Dokshitzer-Gribov-Lipatov-Altarelli-Parisi) evolution. Studies along this line not only confirm HERA investigations but also provide crucial benchmarks for further investigations of the high-energy limit of QCD at the Electron-Ion Collider (EIC) [6] and the large Hadron Electron Collider (LHeC) [7,8]. The kinematic extension of the LHeC will allow us to examine the non-linear dynamics at low x . The non-linear region is approached when the reaction is mediated by multi-gluon exchange. Indeed the growth of the gluon density is slowed down at very small x by gluon-gluon recombination process. The kinematic coverage of the NC e^-p scattering pseudodata at the LHeC which indicate the nonlinear dynamics are defined in the region $x < 0.01$ and $Q^2 < 700 \text{ GeV}^2$ [9,10]. At small x the effect of $\propto \ln(1/x)$ terms on the linear evolution equations increases. So nonlinear interactions must be applied. Indeed we need reliable LHeC predictions to understand the low x physics [11]. Since non-linear dynamics are

*Electronic address: grboroun@gmail.com; boroun@razi.ac.ir

†brezaei@razi.ac.ir

known to become sizable only at small- x , so the nonlinear contribution to the evolution equation [12] leads to an equation of the form

$$\frac{\partial^2 xg(x, Q^2)}{\partial \ln(1/x) \partial \ln Q^2} = \bar{\alpha}_s xg(x, Q^2) - \frac{9}{16} \bar{\alpha}_s^2 \pi^2 \frac{[xg(x, Q^2)]^2}{\mathcal{R}^2 Q^2}, \quad (4)$$

where $\bar{\alpha}_s \equiv \alpha_s C_A / \pi$ and the parameter \mathcal{R} controls the strength of the nonlinearity. The second nonlinear term in (4) is responsible for gluon recombination. This term arises from perturbative QCD diagrams which couple four gluons to two gluons. So that two gluon ladders recombine into a single gluon ladder. It leads to saturation of the gluon density at low Q^2 with decreasing x [13]. The gluon recombination is as important as gluon splitting which in analysis some groups such as MRST2001 [14] and CETQ6M [15] in NLO analysis considered. This implies that towards small values of x and Q^2 , the problem of negative gluon distribution in these groups appears. Other non-linear equations such as Modified-DGLAP (Md-DGLAP) [16], Balitsky-Kovchegov (BK) [17] and Jalilian-Marian-McLerran-Weigert-Leonidov-Kovner (JIMWLK) [18] equations have been derived and considered in the last years. Some another models, such as the impact-parameter dependent saturation model (IP-Sat) [9], developed a dipole model for DESY HERA which incorporates the impact parameter distribution of the proton. It is a simple dipole model that incorporates key features of the physics of gluon saturation. This model for the dipole amplitude contains an eikonalized gluon distribution which satisfies DGLAP evolution while explicitly maintaining unitarity [19]. In Ref.[20] the nonlinear evolution equation for dipole density have been developed. The deeply inelastic scattering at very high energies in the saturation regime considered. The unitarity problem is discussed in Ref.[21] with respect to photoabsorption cross sections. The unitarity relation entails the nonlinearity of the observed DIS structure functions in terms of the impulse approximation (IA) parton densities. The expectation value of the interaction cross sections of the multiparton Fock states of the virtual photon over the wave functions is considered in [21]. The unitarized total cross sections $\sigma(x, \rho)$ reads

$$\sigma(x, \rho) \simeq \sigma_0(x, \rho) \text{ at } \eta(x, \rho) \ll 1$$

where the quantity $\eta(x, \rho)$ controls the effect of the unitarization and ρ is the transverse size of the $q\bar{q}$ pair. At $\eta(x, \rho) \gg 1$ the unitarization suppresses the cross section as $\sigma(x, \rho) \ll \sigma_0(x, \rho)$ where $\sigma_0(x, \rho)$ is the interaction cross section for the $q\bar{q}$ color dipole of size ρ . The effects of the $q\bar{q}g$ Fock state is deriving term of the triple-pomeron mass spectrum. The shadowing term in the unitarized structure function is dominated by the triple-pomeron term, which is approximately independent of the flavor and Q^2 variables. Indeed the unitarity (shadowing) correction is a nonlinear functional of the

DGLAP cross section. Also the unitarity correction can be related to the cross section of the forward diffractive dissociation of the virtual photons (DDIS) $\gamma^* + p \rightarrow X + p$ where $X = q\bar{q}$. The conventional description of DDIS is based on the leading twist DGLAP evolution equations which characterize the QCD hard scale dependence of the diffractive parton distribution functions (DPDFs) [22]. The effects of pomeron loops and running coupling on the cross sections for inclusive $\gamma^* h$ and on diffractive deep inelastic scattering are investigated in Ref.[23]. In Ref.[24] DDIS provides a basis for the definition of the Weizsäcker-Williams (WW) nuclear gluon structure function. Also the initial conditions at low x DIS off nucleons and nuclei for QCD evolution that satisfy unitarity are described. The nonlinear effects can be tested at a superior statistical accuracy attainable at EIC.

This paper is organized as follows. In the next section the theoretical formalism is presented, including the nonlinear evolution and the color dipole parameters. In section 3, we present a detailed numerical analysis and our main results. We then confront these results with the CDM bounds at low values of Q^2 . In the last section we summarize our main conclusions and remarks.

2. Theoretical formalism

In the CDM the ρ parameter is dependent on the proton structure function $F_2(x, Q^2)$ and the gluon distribution function $G(x, Q^2)$ as reads

$$\rho(x, Q^2) = \frac{27\pi}{20\alpha_s(Q^2)} \frac{F_2(x, Q^2)}{G(x, Q^2)} - \frac{1}{2}. \quad (5)$$

An analytical expression for $F_2(x, Q^2)$ has suggested which describes fairly well the available experimental data on the reduced cross section [25]. This parameterization provides reliable structure function $F_2(x, Q^2)$ according to HERA data at low x in a wide range of the momentum transfer ($1 \text{ GeV}^2 < Q^2 < 3000 \text{ GeV}^2$) as

$$F_2(x, Q^2) = D(Q^2)(1-x)^n \sum_{m=0}^2 A_m(Q^2) L^m, \quad (6)$$

and can be applied as well in analyses of ultra-high energy processes with cosmic neutrinos. In a new method, the linear behavior of the gluon density in the CDM parameters is investigated in Ref.[26]. Now we consider the nonlinear behavior of the gluon density for the CDM bounds. The nonlinear effects of the gluon-gluon fusion due to the high gluon density at small x is considered in Gribov-Levin-Ryskin-Mueller-Qiu (GLR-MQ) [12]. Some studies of the GLR-MQ equation in the framework of the extracting the gluon distribution function have been discussed

considerably over the past years [27-33]. The GLR-MQ equation can be written in standard form [34]

$$\frac{\partial G(x, Q^2)}{\partial \ln Q^2} = \frac{\partial G(x, Q^2)}{\partial \ln Q^2} \Big|_{DGLAP} - \frac{81}{16} \frac{\alpha_s^2(Q^2)}{\mathcal{R}^2 Q^2} \int_{\chi}^1 \frac{dz}{z} G^2\left(\frac{x}{z}, Q^2\right), \quad (7)$$

where $\chi = \frac{x}{x_0}$ and x_0 is the boundary condition that the gluon distribution joints smoothly onto the linear region. The correlation length \mathcal{R} determines the size of the nonlinear terms. This value depends on how the gluon ladders are coupled to the nucleon or on how the gluons are distributed within the nucleon. The \mathcal{R} is approximately equal to $\simeq 5 \text{ GeV}^{-1}$ if the gluons are populated across the proton and it is equal to $\simeq 2 \text{ GeV}^{-1}$ if the gluons have hotspot like structure. By solving GLR-MQ (Eq.7), we obtain an expression for the nonlinear gluon distribution function (i.e., $G^{\text{NL}}(x, Q^2)$) as

$$G^{\text{NL}}(x, Q^2) = G^{\text{NL}}(x, Q_0^2) + G(x, Q^2) - G(x, Q_0^2) - \int_{Q_0^2}^{Q^2} \frac{81}{16} \frac{\alpha_s^2(Q^2)}{\mathcal{R}^2 Q^2} \int_{\chi}^1 \frac{dz}{z} G^2\left(\frac{x}{z}, Q^2\right) d \ln Q^2 \quad (8)$$

We note that at $x \geq x_0 (= 10^{-2})$ the linear and nonlinear gluon distribution behaviors are equal. At Q_0^2 the low x behavior of the nonlinear gluon distribution is assumed to be [35]

$$G^{\text{NL}}(x, Q_0^2) = G(x, Q_0^2) \left\{ 1 + \frac{27\pi\alpha_s(Q_0^2)}{16\mathcal{R}^2 Q_0^2} \theta(x_0 - x) \times [G(x, Q_0^2) - G(x_0, Q_0^2)] \right\}^{-1}. \quad (9)$$

Substituting Eqs.(6) and (8) in Eq.(5) the nonlinear behavior of the ρ parameter becomes

$$\rho^{\text{NL}}(x, Q^2) = \frac{27\pi}{20\alpha_s(Q^2)} \frac{F_2(x, Q^2)(i.e., Eq.(6))}{G^{\text{NL}}(x, Q^2)(i.e., Eq.8)} - \frac{1}{2} \quad (10)$$

Next we define the nonlinear behavior of the longitudinal-to-transverse cross sections and the structure functions by the following forms respectively

$$R^{\text{NL}}(W^2, Q^2) = \frac{1}{2\rho^{\text{NL}}(W^2, Q^2)}, \quad (11)$$

and

$$F_{L/2}^{\text{NL}}(W^2, Q^2) \equiv \frac{F_L(W^2, Q^2)}{F_2(W^2, Q^2)} = \frac{1}{1 + 2\rho^{\text{NL}}(W^2, Q^2)} \quad (12)$$

If we rewrite the reduced cross section in terms of the nonlinear behavior of the ratio of the structure functions, then the nonlinear behavior of the reduced cross section at low Q^2 reads

$$\sigma_r^{\text{NL}}(W^2, Q^2) = F_2(W^2, Q^2) \left[1 - \frac{y^2}{1 + (1 - y)^2} \times \frac{1}{1 + 2\rho^{\text{NL}}(W^2, Q^2)} \right]. \quad (13)$$

Here $W^2 \simeq sy$ which the inelasticity y is related to Q^2 , x and the center-of-mass energy squared, $s = 4E_e E_p$, by $y = Q^2/sx$.

In the following we consider the deeply inelastic structure functions at low Q^2 using the higher-twist (HT) corrections in QCD. Using this effect in the parameterization of the proton structure function is expected to provide better results for the reduced cross section than the experimental data. The higher-twist corrections arise from the struck proton's interaction with target remnants where reflecting confinement [36-40]. The phenomenological power correction to the structure function from the HT corrections is considered by the following form

$$F_2^{\text{HT}}(x, Q^2) = F_2^{\text{Parameterization}}(x, Q^2) \left(1 + \frac{C_{HT}(x)}{Q^2} \right) \quad (14)$$

which the coefficient function $C_{HT}(x)$ is determined from fit to the data. In some references [37-41] this quantity is set to be an free parameter as $C_{HT} = 0.12 \pm 0.07 \text{ GeV}^2$ and in others [42,43] it depends on x as

$$C_{HT}(x) = h_0(h_2(x)x^{h_1} + \gamma).$$

In Refs.[42,43] this fit parameterization is obtained from the QCD analysis with the HT corrections included. Therefore it is clear from Eqs.(13) and (14) that at low Q^2 , we can add the HT corrections and our solution takes the form

$$\sigma_r^{\text{NL+HT}}(W^2, Q^2) = F_2^{\text{HT}}(W^2, Q^2) \left[1 - \frac{y^2}{1 + (1 - y)^2} \times \frac{1}{1 + 2\rho^{\text{NL+HT}}(W^2, Q^2)} \right], \quad (15)$$

with

$$\rho^{\text{NL+HT}}(x, Q^2) = \frac{27\pi}{20\alpha_s(Q^2)} \frac{F_2^{\text{HT}}(x, Q^2)}{G^{\text{NL}}(x, Q^2)} - \frac{1}{2}. \quad (16)$$

3. Results and discussions

In this paper, we obtain the nonlinear gluon distribution function solving the GLR-MQ evolution equation for gluon density. The analysis is performed in the range $10^{-5} \leq x \leq 10^{-2}$ and $1 \leq Q^2 \leq 100 \text{ GeV}^2$. The computed results of nonlinear gluon distribution function are compared with the CDP model [5] (Kuroda and Schildknecht, Phys.Rev.D85, 094001(2011)) and the parameterization model [25] in Fig.1. According to Fig.7 in Ref.[5] (Kuroda and Schildknecht, Phys.Rev.D85, 094001(2011)), there is a considerable agreement to the results from the CETQ [44] and MSTW [45] collaborations. The nonlinear gluon distribution behavior is comparable with MSTW08 NNLO [46] at $Q^2 > 1 \text{ GeV}^2$.

In the following, the parameters and bounds with respect

to the nonlinear gluon distribution behavior can be examined. With the obtained ρ parameter, we calculate the ratio of structure functions and also the reduced cross sections with respect to the nonlinear and higher twist corrections. These functions are obtained at low x and Q^2 values by taking an appropriate input parton distribution. In Fig.2, the parameters ρ , R and $F_{L/2}$ are obtained with respect to the nonlinear behavior of the gluon distribution function. In the following we have investigated the effect of nonlinearity in our results in the hot-spot point. The value of this parameter is defined to be $R = 2 \text{ GeV}^{-1}$ in this work. In Fig.2 we shown that the nonlinear results are much closer to the color dipole bounds than the linear ones. The comparison is for $Q^2 = 5 \text{ GeV}^2$ and $Q^2 = 10 \text{ GeV}^2$. The fluctuations corresponding to the parameters (i.e., ρ , R and $F_{L/2}$) in comparison with constant CDM bounds are due to the parameterization of the PDFs. By adding the effect of the HT corrections on the parameters, we showed that the results have a behavior comparable to the CDM bounds. In Fig.3, a comparison for $Q^2 = 5 \text{ GeV}^2$ has been made between the nonlinear and nonlinear+higher twist (NL+HT) corrections to the parameters. In the following we will apply these corrections (i.e., NL+HT) to all results. As can be observe in Fig.4, the ratio of the structure functions are comparable to the H1 data [47] and CDM bounds [3,4,48] not only at large Q^2 but also at low Q^2 values. Indeed, the transition from the linear to nonlinear is done due to the nonlinear corrections to the gluon distribution function. Compared to other results and models, we see that the ratio F_L/F_2 is in fact comparable to the results of others [10,49] and experimental data. This comparison is very good at low and high- Q^2 values, even compared to other models such as Golec-Biernat-Wüsthoff (GBW)[10] and Iancu-Itakura-Munier (IIM) [49] parameterizations. The nonlinear behavior of the ratio of structure functions at low Q^2 in Fig.5 is observable in comparison with the H1 data [41]. In Fig.5, data collected in the region of low momentum transfers, $0.2 \text{ GeV}^2 \leq Q^2 \leq 12 \text{ GeV}^2$, and low Bjorken x , $10^{-6} \lesssim x \lesssim 0.02$ with center-of-mass energy $\sqrt{s} = 319 \text{ GeV}$. In Ref.[41] the structure functions of F_2 and F_L collected without the total errors. Tables 17 and 18 in this reference shown that F_L^{th} represents the structure function F_L used for the center-of-mass energy (CME) correction and to calculate the structure function F_2 . Therefore we compared our results at $x=0.001$ in a wide range of W^2 between 10^3 GeV^2 and 10^4 GeV^2 with the ratio of structure functions (i.e., H1 2009 [41]) without the total uncertainties in Fig.5.

In the following we use the NL+HT behavior of the ratio F_L/F_2 to calculate the reduced cross section. In Ref.[41] the H1 collaboration reported the DIS cross sections at low Q^2 . The DIS data collected based on the SVX, NVX-BST and NVX-S9 analysis [41]. We use the SVX data at $Q^2 = 2 \text{ GeV}^2$, the NVX-BST and NVX-S9 data at $Q^2 = 5 \text{ GeV}^2$ and the NVX-BST data at $Q^2 = 12 \text{ GeV}^2$.

The cross section data due to the NL+HT effects at three values of Q^2 are given in Table I, and compared with the H1 data [41] measured from the SVX and NVX data. Here we discuss the χ^2 method for comparison according to the number of points at any Q^2 values. The χ^2 can be defined as

$$\chi^2 = \sum_i^{N_{\text{data}}} (X_{\text{data},i} - X_{\text{method},i})^2 / (\delta X_i)^2, \quad (17)$$

where i runs all the data points, δX_i can be the total experimental uncertainties. The χ^2/N_{data} can quantify the agreement between the data and our predictions. The χ^2/N_{data} computed at different values of Q^2 is in Table II. The results are plotted in Fig.6. In this figure, together with the H1 data [41], we plot the x dependence of the reduced cross section $\sigma_r(x, Q^2)$ computed with respect to the nonlinear and higher-twist effects for fixed values of Q^2 . The error bands are in accordance with the statistical errors of the parameterization of F_2 and the errors bars are quoted in % relative to σ_r . The agreement of these results with the H1 data are excellent for $x < 0.01$. We also compare these results with the HERA data [50] (which combines H1 and ZEUS data) in Fig.6 at Q^2 values of 2 and 12 GeV^2 . This includes data taken with proton beam energies of $E_p = 920 \text{ GeV}$ corresponding to the center-of-mass energy $\sqrt{s} = 318 \text{ GeV}$. Therefore, the results of the current paper in the region of smallest x and Q^2 studies can confirm the nonlinear corrections to the small- x gluon distributions for transition.

4. Summary

In conclusion, we have studied the effects of adding the nonlinear corrections to the gluon density for transition from the linear to the nonlinear regions. We use the parameterization of $F_2(x, Q^2)$ as a baseline. This analysis is also enriched with the higher twist (HT) contributions to the proton structure function at small values of Q^2 . The nonlinear and higher twist corrections to the ratio of structure functions and also to the reduced cross sections are considered. Comparing these parameters with the CDM bounds indicate that the NL+HT effects are enriched the behavior at low Q^2 . The transition of the ratio $F_{L/2}$ from the linear to the nonlinear behavior is considered and shown that it is in good agreement with the CDM bounds non only at high- Q^2 but also at low- Q^2 values. Comparison of the reduced cross sections with respect to the nonlinear and higher twist corrections with HERA data at low and moderate Q^2 values shows that this transition has been done with good accuracy in comparison with the HERA data.

ACKNOWLEDGMENTS

Authors are grateful the Razi University for financial support of this project. G.R.Boroun is especially grateful to D.Schildknecht for carefully reading the manuscript and fruitful discussions.

REFERENCES

1. J.J.Sakurai and D.Schildknecht, *Phys.Lett.***B40**, 121(1972); B.Gorczyca and D.Schildknecht, *Phys.Lett.***B47**, 71(1973).
2. N.N.Nikolaev and B.G.Zakharov, *Z.Phys.***C49**, 607(1991); *Z.Phys.***C53**, 331(1992); A.H.Mueller, *Nucl.Phys.***B415**, 373(1994); K.Golec-Biernat and M.Wüsthoff, *Phys.Rev.***D59**, 014017(1998); H.Kowalski, L.Motyka and G.Watt, *Phys.Rev.***D74**, 074016(2006); B.Sambasivam, T.Toll and T.Ullrich; *Phys.Lett.***B803**, 135277(2020); G.M.Peccini, F.Kopp, M.V.T.Machado and D.A.Fagundes, *Phys.Rev.***D101**, 074042 (2020).
3. M.Kuroda and D.Schildknecht, *Phys.Lett.* **B618**, 84(2005); M.Kuroda and D.Schildknecht, *Phys.Rev.* **D96**, 094013(2017); D.Schildknecht, B.Surrow and M.Tentyukov, *Eur.Phys.J.***C20**, 77(2001); M.Kuroda and D.Schildknecht, *International Journal of Modern Physics* **A31**, No. 30, 1650157 (2016).
4. D.Schildknecht, *Nuclear Physics B Proceedings Supplement* 146, 211 (2005) ; *Nuclear Physics B Proceedings Supplement* 00, 1 (2012); F.Schrempp and A.Utermann, *Acta Phys.Polon.***B33**, 3633(2002).
5. M.Kuroda and D.Schildknecht, *Phys.Lett.* **B670**, 129(2008); M.Kuroda and D.Schildknecht, *Phys.Rev.***D85**, 094001(2011).
6. D.Boer et al., arXiv: [nucl-th]1108.1713.
7. J.Abelleira Fernandez et al., [LHeC Study Group Collaboration], *J.Phys.***G39**, 075001(2012); A. Abada et al., [FCC Study Group Collaboration], *Eur.Phys.J.***C79**, 474(2019).
8. P.Agostini et al. [LHeC Collaboration and FCC-he Study Group], CERN-ACC-Note-2020-0002, arXiv:2007.14491 [hep-ex] (2020).
9. H.Kowalski and D.Teaney, *Phys.Rev.***D68**, 114005(2003); G.Watt and H.Kowalski, *Phys.Rev.***D78**, 014016(2008).
10. J.Bartels, K.Golec-Biernat and H.Kowalski, *Phys.Rev.***D66**, 014001(2002); K.Golec-Biernat and M.Wüsthoff, *Phys.Rev.***D60**, 114023(1999); K.Golec-Biernat and S.Sapeta, *J.High Energ.Phys.***03**, 102(2018).
11. M.Klein, arXiv [hep-ph]:1802.04317; M.Klein, *Ann.Phys.***528**, 138(2016); N.Armeesto et al., *Phys.Rev.***D100**, 074022(2019).
12. L.V.Gribov, E.M.Levin and M.G.Ryskin, *Phys.Rept.***100**, 1(1983); A.H.Mueller and J.w.Qiu, *Nucl.Phys.***B268**, 427(1986).
13. M.R.Pelicer et al., *Eur.Phys.J.***C79**, 9(2019).
14. A.D.Martin, R.G.Roberts, W.J.Stirling and R.S.Thorne, *Eur.Phys.J.***C23**, 73(2002); *Phys.Lett.***B531**, 216(2002).
15. J.Pumplin et al., *J.High Energ.Phys.***07**, 012(2002).
16. W.Zhu, J.Ruan, J.Yang and Z.Shen, *Phys.rev.***D68**, 094015(2003).
17. I.Balitsky, *Nucl.Phys.***B463**, 99(1996);

- Y.V.Kovchegov, *phys.Rev.D***60**, 034008(1999).
18. J.Jalilian-Marian, A.Kovner, a.Leonidov and H.Weigert, *Nucl.Phys.B***504**, 415(1997); *Phys.Rev.D***59**, 014014(1998); E.Iancu, A.Leonidov and L.D.McLerran, *Nucl.Phys.A***692**, 583(2001); *Nucl.Phys.A***703**, 489(2002).
 19. A.H.Rezaeian et al., *Phys.Rev.D***87**, 034002(2013).
 20. I.I.Balitsky and A.V.Belitsky, *Nucl.Phys.B***629**, 290(2002).
 21. V. Barone et al., *Phys.Lett.B***326**, 161(1994).
 22. M. Sadzikowski, L. Motyka and W. Slominski, arXiv [hep-ph]:1206.1732 (2012).
 23. M.B.Gay Ducati, E.G.de Oliveira and J.T.de Santana Amaral, arXiv [hep-ph]:1209.5354 (2012).
 24. I.P.Ivanov et al., XXXII International Symposium on Multiparticle Dynamics, pp. 169-176 (2003); K.Tywniuk, *Journal of Physics: Conference Series***270**, 012054 (2011).
 25. M. M. Block, L. Durand and P. Ha, *Phys. Rev.D***89**, no. 9, 094027 (2014).
 26. G.R. Boroun, arXiv:2102.04867 (2021).
 27. M.Devee and J.K.Sarma, *Eur.Phys.J.C***74**, 2751(2014); *Nucl.Phys.B***885**, 571(2014); P.Phukan, M.Lalung and J.K.Sarma, *Nucl.Phys.A***968**, 275(2017); M.Lalung, P.Phukan and J.K.Sarma, *Nucl.Phys.A* **992**, 121615(2019); M.Devee, arXiv:1808.00899 [hep-ph] (2018); P.Gilvana and S.K.Werner, arXiv:1804.10659 [hep-ph] (2018).
 28. G.R.Boroun, *Eur.Phys.J.A***42**, 251(2009).
 29. G.R.Boroun, *Phys.Rev.C***97**, 015206(2018).
 30. B.Rezaei and G.R.Boroun, *Phys.Rev.C***101**, 045202(2020).
 31. B.Rezaei and G.R.Boroun, *Eur.Phys.J.A***56**, 262(2020).
 32. G.R.Boroun and S.Zarrin, *Eur.Phys.J.Plus***128**, 119(2013).
 33. G.R.Boroun and B.Rezaei, *Nucl.Phys.A***1006**, 122062 (2021).
 34. K.Prytz, *Eur.Phys.J.C***22**, 317(2001); K.J.Eskola et al., *Nucl.Phys.B***660**, 211(2003); M.A Kimber, J.Kwiecinski and A.D.Martin, *Phys.Lett.B***508**, 58(2001).
 35. A.D.Martin et al., *Phys.Rev.D***47**, 867(1993); J.Kwiecinski, A.D.Martin and P.J.Sutton, *Phys.Rev.D***44**, 2640(1991); A.J.Askew, J.Kwiecinski, A.D.Martin and P.J.Sutton, *Phys.Rev.D***47**, 3775(1993).
 36. B.Badelek et al., *J.Phys.G***22**, 815(1996); S. Catani and F. Hautmann, *Nucl.Phys.B***427**, 475(1994); J.Blumlein and H.Bottcher, arXiv[hep-ph]:0807.0248(2008).
 37. A.M.Cooper-Sarkar et al., arXiv:1605.08577v1 [hep-ph] 27 May 2016.
 38. I.Abt et.al., *Phys.Rev.D***94**, 034032(2016).
 39. G.R.Boroun and B.Rezaei, *Phys.Lett.B***816**, 136274 (2021).
 40. G.R.Boroun and B.Rezaei, *Nucl.Phys.A***990**, 244(2019).
 41. F.D. Aaron et al. [H1 Collaboration], *Eur.Phys.J.C***63**, 625(2009).
 42. H.Khanpour, A.Mirjalili and S.Atashbar Tehrani, *Phys.Rev.C***95**, 035201 (2017).
 43. H.Khanpour, *Phys.Rev.D***99**, 054007(2019).
 44. J. Pumplin et al., [CTEQ Collaboration] *JHEP***0207**, 012(2002).
 45. A.D. Martin et al., *Eur. Phys. J. C***18**, 117(2000).
 46. A.D. Martin et al., *Eur. Phys. J. C***63**, 189(2009).
 47. V.Andreev et al. [H1 Collaboration], *Eur.Phys.J.C***74**, 2814(2014).
 48. C.Ewerz, A.von Manteuffel and O.Nachtmann, *JHEP***03**, 102(2010); D.Britzger et al., *Phys.Rev.D***100**, 114007 (2019); C.Ewerz, A. von Manteuffel and O.Nachtmann, *Phys.Rev.D***77**, 074022(2008); C.Ewerz and O.Nachtmann, *Phys.Lett.B***648**, 279 (2007).
 49. E.Iancu,K.Itakura and S.Munier, *Phys.Lett.B***590**, 199(2004); M.Niedziela and M.Praszalowicz, *Acta Physica Polonica B***46**, 2018(2015).
 50. H.Abramowicz et al., [H1 and ZEUS Collaborations], *Eur.Phys.J.C***75**, 580(2015).

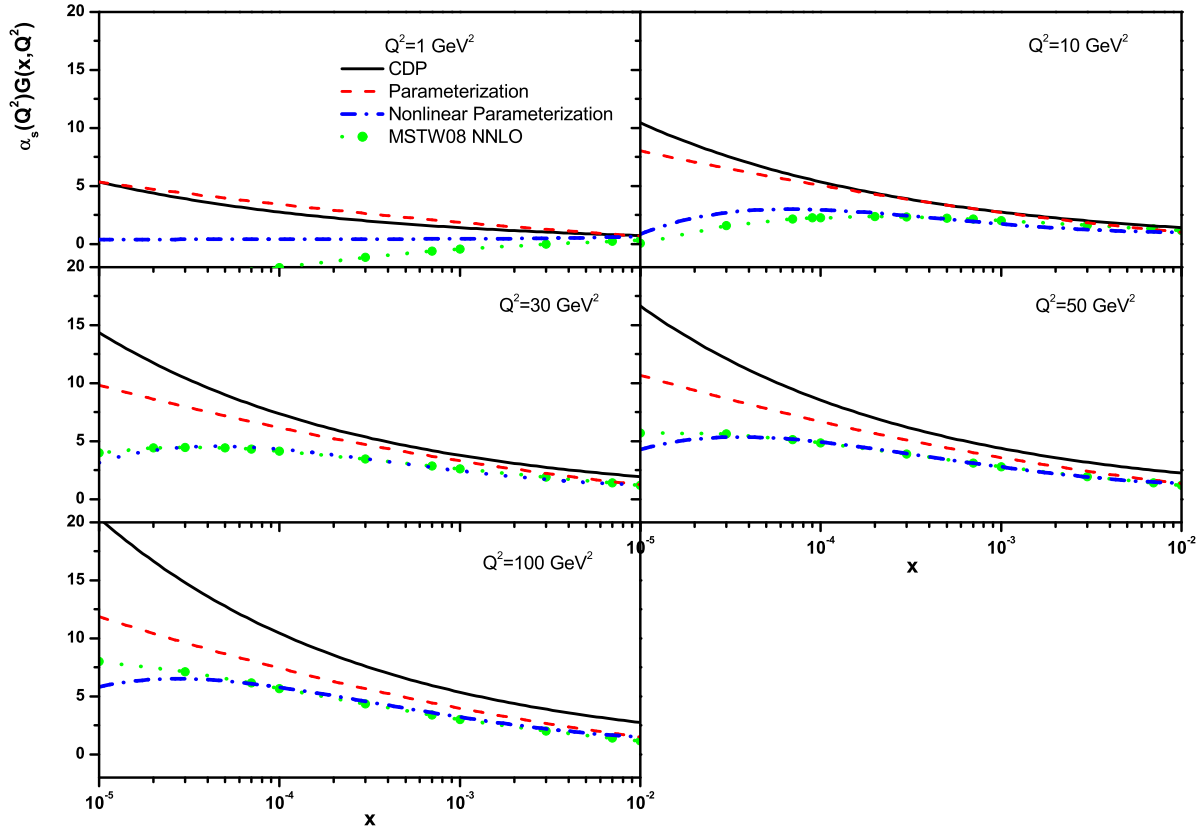


FIG. 1: The nonlinear gluon distribution function at $R = 2 \text{ GeV}^{-1}$ compared with the gluon distributions from the CDP model [5] (Kuroda and Schildknecht, Phys.Rev.D85, 094001(2011)), the parameterization model [25] and MSTW08 NNLO [46].

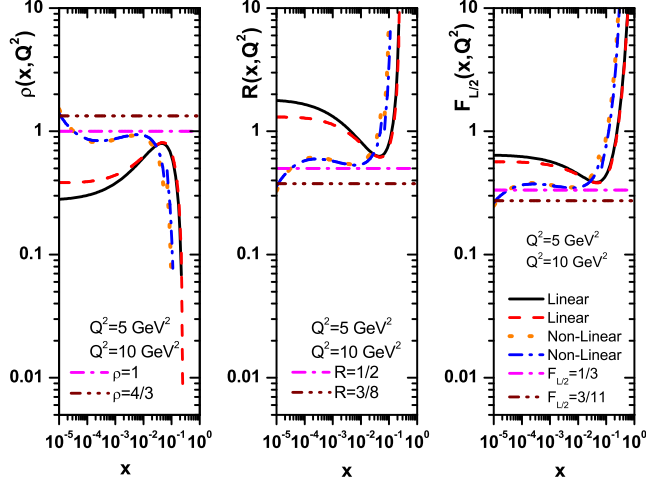


FIG. 2: Results of the parameters (a) : $\rho(x, Q^2)$, (b) : $R(x, Q^2)$ and (c) : $F_{L/2}(x, Q^2)$ obtained from the linear and nonlinear corrections at fixed Q^2 values ($Q^2 = 5 \text{ GeV}^2$, Black-linear and Orange-nonlinear; $Q^2 = 10 \text{ GeV}^2$, Red-linear and Blue-nonlinear) respectively. The parameters compared with the CDP bounds in (a) : $\rho = 1$ and $4/3$, in (b) : $R = 1/2$ and $3/8$ and in (c) : $F_{L/2} = 1/3$ and $3/11$ respectively.

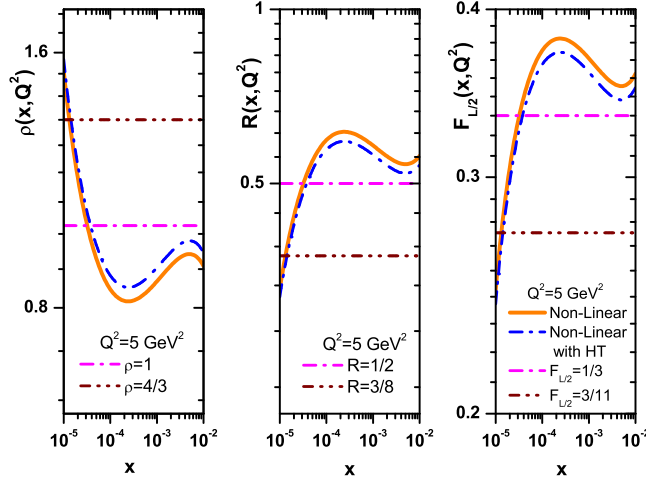


FIG. 3: Comparison of the nonlinear behavior of the parameters (a) : $\rho(x, Q^2)$, (b) : $R(x, Q^2)$ and (c) : $F_{L/2}(x, Q^2)$ with the higher-twist corrections at $Q^2 = 5 \text{ GeV}^2$. The parameters compared with the CDP bounds in (a) : $\rho = 1$ and $4/3$, in (b) : $R = 1/2$ and $3/8$ and in (c) : $F_{L/2} = 1/3$ and $3/11$ respectively.

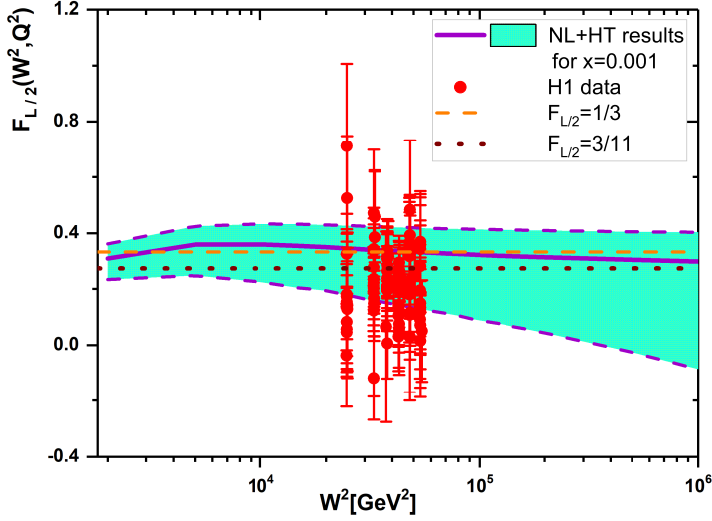


FIG. 4: The ratio of the longitudinal to transversal structure functions calculated due to the nonlinear and higher twist effects at fixed value of the Bjorken variable $x = 0.001$. Experimental data are from the H1 Collaboration as accompanied with total errors [47]. The obtained values compared with the CDP bounds [3,4,48] $F_{L/2} = 1/3$ and $3/11$. The error bands are due to the effective parameters in the parameterization of $F_2(x, Q^2)$ [25] and also the HT coefficient errors [36-40,42,43].

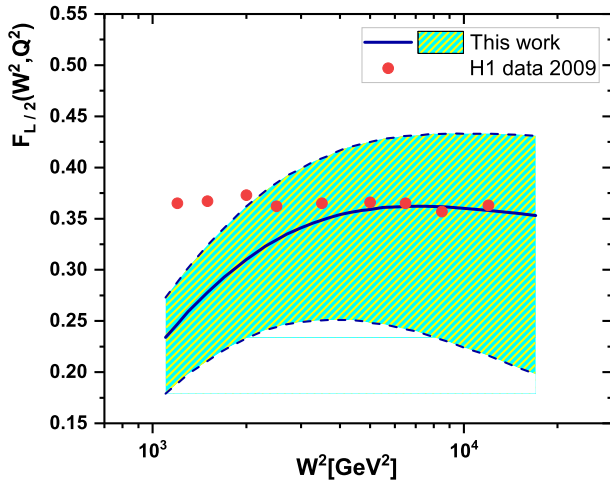


FIG. 5: Continue Fig.3 in the low Q^2 values. The ratio of the longitudinal to transversal structure functions calculated due to the nonlinear and higher twist effects at fixed value of the Bjorken variable $x = 0.001$. Data are from the H1 Collaboration [41] without the total uncertainties at low Q^2 . The error bands are due to the effective parameters in the parameterization of $F_2(x, Q^2)$ [25] and also the HT coefficient errors [36-40,42,43].

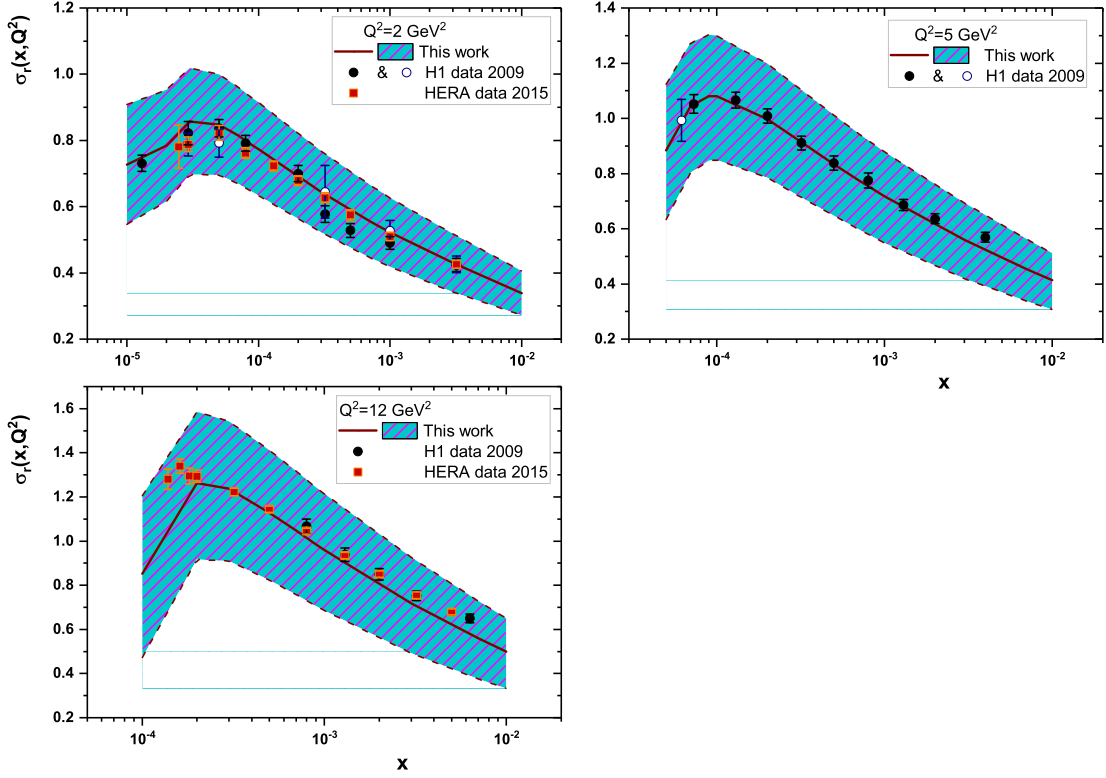


FIG. 6: Reduced cross section σ_r^{NL+HT} from the nonlinear behavior of the gluon distribution and the higher twist corrections to the proton structure function at low x and Q^2 compared to the reduced cross section σ_r from the combined low Q^2 data [41] and also HERA combined data [50]. H1 data accompanied with total errors. H1 data represented for $Q^2 = 2 \text{ GeV}^2$ as the closed circles are SVX data, and the open circles are NVX-BST data, for $Q^2 = 5 \text{ GeV}^2$ the closed circles are NVX-BST data and the open circles are NVX-S9 data, and also for $Q^2 = 12 \text{ GeV}^2$ the closed circles are NVX-BST data [41]. The error bands are due to the effective parameters in the parameterization of $F_2(x, Q^2)$ [25] and also the HT coefficient errors [36-40,42,43]. This comparison with HERA combined data [50] at $Q^2 = 2$ and 12 GeV^2 is defined.

TABLE I: The reduced cross section σ_r , determined based on the nonlinear and higher twist effects in Q^2 values 2, 5 and 12 GeV^2 at $x < 0.01$. These results accompanied with the uncertainties due to the coefficient functions errors [25] and compared with the H1 data [41] as the uncertainties are quoted in % relative to σ_r .

$Q^2(\text{GeV}^2)$	x	H1 data	$\sigma_r \pm \delta\%$	$\sigma_r \pm \delta$
2	2.470E-5	NVX – S9 data	$0.756 \pm 9.23\%$	$0.833^{+0.165}_{-0.164}$
2	2.928E-5	SVX data	$0.822 \pm 4.28\%$	$0.855^{+0.161}_{-0.161}$
2	2.928E-5	NVX – BST data	$0.788 \pm 4.45\%$	$0.855^{+0.161}_{-0.161}$
2	5.000E-5	SVX data	$0.837 \pm 3.10\%$	$0.847^{+0.152}_{-0.151}$
2	5.000E-5	NVX – BST data	$0.792 \pm 5.31\%$	$0.847^{+0.152}_{-0.151}$
2	8.000E-5	SVX data	$0.791 \pm 3.03\%$	$0.800^{+0.144}_{-0.143}$
2	1.300E-4	SVX data	$0.731 \pm 3.28\%$	$0.742^{+0.136}_{-0.135}$
2	2.000E-4	SVX data	$0.700 \pm 3.58\%$	$0.691^{+0.129}_{-0.129}$
2	3.200E-4	SVX data	$0.578 \pm 4.39\%$	$0.637^{+0.121}_{-0.121}$
2	3.200E-4	NVX – BST data	$0.645 \pm 12.2\%$	$0.637^{+0.121}_{-0.121}$
2	5.000E-4	SVX data	$0.528 \pm 3.95\%$	$0.590^{+0.116}_{-0.115}$
2	1.000E-3	SVX data	$0.490 \pm 3.79\%$	$0.523^{+0.104}_{-0.104}$
2	1.000E-3	NVX – BST data	$0.527 \pm 5.93\%$	$0.523^{+0.104}_{-0.104}$
2	3.200E-3	SVX data	$0.424 \pm 4.65\%$	$0.425^{+0.087}_{-0.087}$
2	3.200E-3	NVX – BST data	$0.426 \pm 5.80\%$	$0.425^{+0.087}_{-0.087}$
5	6.176E-5	NVX – S9 data	$0.933 \pm 7.70\%$	$1.002^{+0.233}_{-0.244}$
5	7.320E-5	NVX – BST data	$1.052 \pm 3.26\%$	$1.055^{+0.228}_{-0.240}$
5	1.300E-4	NVX – BST data	$1.066 \pm 2.72\%$	$1.062^{+0.212}_{-0.223}$
5	2.000E-4	NVX – BST data	$1.009 \pm 2.62\%$	$0.997^{+0.201}_{-0.212}$
5	3.200E-4	NVX – BST data	$0.911 \pm 2.79\%$	$0.913^{+0.190}_{-0.199}$
5	5.000E-4	NVX – BST data	$0.838 \pm 3.11\%$	$0.834^{+0.178}_{-0.187}$
5	8.000E-4	NVX – BST data	$0.775 \pm 3.50\%$	$0.754^{+0.166}_{-0.175}$
5	1.300E-3	NVX – BST data	$0.686 \pm 2.91\%$	$0.677^{+0.154}_{-0.162}$
5	2.000E-3	NVX – BST data	$0.636 \pm 2.84\%$	$0.615^{+0.143}_{-0.151}$
5	3.980E-3	NVX – BST data	$0.569 \pm 3.18\%$	$0.523^{+0.125}_{-0.133}$
12	8.000E-4	NVX – BST data	$1.067 \pm 3.05\%$	$1.014^{+0.263}_{-0.284}$
12	1.300E-3	NVX – BST data	$0.938 \pm 3.31\%$	$0.898^{+0.243}_{-0.262}$
12	2.000E-3	NVX – BST data	$0.850 \pm 3.00\%$	$0.802^{+0.224}_{-0.243}$
12	3.200E-3	NVX – BST data	$0.752 \pm 2.98\%$	$0.705^{+0.205}_{-0.222}$
12	6.310E-3	NVX – BST data	$0.650 \pm 2.89\%$	$0.578^{+0.174}_{-0.190}$

TABLE II: The values of χ^2/N for the computed σ_r to the H1 data [41] in the small and moderate- Q^2 regions for $x < 0.01$ are determined. Also the number of data points in each case is mentioned.

$Q^2(\text{GeV}^2)$	H1 data	N	χ^2/N
2	NVX – S9 data	15	1.696
	NVX – BST data		
	SVX data		
5	NVX – S9 data	10	1.021
	NVX – BST data		
12	NVX – BST data	5	5.315